The Influence of Fatty Acid Methyl Ester Profiles on Inter-Cycle Variability in a Heavy Duty Compression Ignition Engine

Phuong X. Pham[(a,*)], Timothy A. Bodisco[(b)], Zoran D. Ristovski[(b)], Richard J. Brown[(b)], Assaad R. Masri[(a)]

[a] *Clean Combustion Research Group, Aerospace, Mechanical and Mechatronic Engineering, The University of Sydney, NSW 2006, Australia*

[b] *Biofuel Engine Research Facility, Queensland University of Technology, Australia*

Abstract

With the advent of alternative fuels, such as biodiesels and related blends, it is important to develop an understanding of their effects on inter-cycle variability which, in turn, influences engine performance as well as its emission. Using four methanol trans-esterified biomass fuels of differing carbon chain length and degree of unsaturation, this paper provides insight into the effect that alternative fuels have on inter-cycle variability. The experiments were conducted with a heavy-duty Cummins, turbo-charged, common-rail compression ignition engine. Combustion performance is reported in terms of the following key in-cylinder parameters: indicated mean effective pressure (IMEP), net heat release rate (NHRR), standard deviation of variability (StDev), coefficient of variation (CoV), peak pressure, peak pressure timing and maximum rate of pressure rise. A link is also established between the cyclic variability and oxygen ratio, which is a good indicator of stoichiometry.

The results show that the fatty acid structures did not have a significant effect on injection timing, injection duration, injection pressure, StDev of IMEP, or the timing of peak motoring and combustion pressures. However, a significant effect was noted on the premixed and diffusion combustion proportions, combustion peak pressure and maximum rate of pressure rise. Additionally, the boost pressure, IMEP and combustion peak pressure were found to be directly correlated to the oxygen ratio. The emission of particles positively correlates with oxygen content in the fuel as well as in the air-fuel mixture resulting in a higher total number of particles per unit of mass.

Key words: Biodiesel, Unsaturation degree, Carbon chain length, Inter-cycle variability, Kernel density estimates

Abbreviations

AFR	Air Fuel Ratio
OR	Oxygen Ratio
OFR	Oxygen Fuel Ratio
FAMEs	Fatty Acid Methyl Esters
Cx:y	x = number of carbon atoms; y = number of double bond
NHRR	Net Heat Release Rate
IMEP	Indicated Mean Effective Pressure
StDev	Standard of Deviation
CoV	Coefficient of Variation
PDFs	Probability Density Functions
Kernel Density	An estimation of the PDFs
DCA	Degree of Crank Angle
TDC	Top Dead Centre
SoI	Start of Injection
SoC	Start of Combustion

1 Introduction

Inter-cycle variability (or combustion variability) resulting mainly from in-cylinder cycle-to-cycle fluctuations in the fuel-air mixture, is a key factor that affects both engine efficiency as well as emissions [1]. A thorough understanding of this phenomenon is now pressing particularly with the advent of biodiesel fuels and blends where variability in the molecular structure of the fuel, due to different feedstocks, could lead to significant inter-cycle variations. Previous studies of combustion variability focused mainly on spark ignition engines and to a lesser extent on compression ignition engines operating with commercial diesel and alternative fuels including LPG and some biodiesels [2–7]. Kouremenos et al. [6] used a single-cylinder diesel engine to study the following key parameters: peak pressure, peak pressure location, maximum rate of pressure rise, and the crank angle at which the maximum rate of pressure rise occurs. This work showed that the fuel pump system has no influence on the cyclic pressure variation. Also using a single-cylinder compression ignition engine, Selim reported an increase in inter-cycle variability

* Corresponding Author: xpha1824@uni.sydney.edu.au

when operating with gaseous dual fuels [5] and a reduction with jojoba methyl ester [7].

Biodiesels are mixtures of fatty acid methyl (or ethyl) esters derived from vegetable oils, animal fat, or algae by transesterification with the aids of methanol (or ethanol) as a solvent to lower the viscosity and surface tension sufficiently to enable adequate atomisation of the sprays in compression ignition engines [8–14]. A key feature of biodiesels, which makes them different from conventional petro-diesel, is the oxygen-bound in the fuels. While there are always two oxygen molecules in one fatty acid methyl ester, the oxygen content in the biofuels depends on the fatty acid ester profile, specifically carbon chain length and unsaturation level.

While oxygen in the fuel can enhance the combustion process, it results in a lower heating value. At the same lambda/equivalence ratio, mixtures of oxygenated fuel and air are always leaner compared to mixtures of hydrocarbon fuels and air [15, 16]. Moser et al. [17] compared blends of ultra low sulfur diesel with 20% of soy bean methyl esters and observed that oxygen in the fuel improves lubricity, increases kinematic viscosity, lowers sulfur content, and results in inferior oxidative stability. In order to account for the oxygen content in the fuel, Muller et al. [15] proposed that the oxygen ratio (OR) and oxygen fuel ratio (OFR) are more appropriate measures of stoichiometry than the standard air to fuel ratio (AFR). The OFR and OR are defined, respectively, as the ratio of total oxygen atoms in the fuels (OFR) or fuels and oxidizers (OR) to the total oxygen atoms required for stoichiometric combustion [15]. Higher oxygen content in a fuel results in a higher oxygen fuel ratio, and also a higher difference between the oxygen ratio and lambda. For instance, the oxygen ratio for hydrocarbon fuels (where OFR=0) is exactly the same as lambda, while in an oxygenated fuel where OFR=0.5, the difference between the oxygen ratio (OR) and lambda is 100% [15]. The differences between the oxygen ratio and lambda for the biodiesels tested here range from 3-7%.

Results from earlier studies of the effects of oxygen content in the biodiesels on combustion efficiency and emission remain controversial [18–23]. Lapuerta et al. [22] and Yuan et al. [23] observed that the presence of oxygen in biodiesels does not lead to increases in NOx formation. However, others [19–21] found that oxygen in the fuels does result in increased NOx, attributable to higher adiabatic flame temperature, as well as reporting increased combustion efficiency and lower soot.

This paper investigates the inter-cycle variability arising from the use of biodiesels and biodiesel blends in a common-rail diesel engine. A range of fatty acid methyl esters, with different carbon chain length and unsaturation degree, are tested as pure fuels as well as blends with commercial diesel. The

oxygen ratio is applied as an indicator of combustion stoichiometry and correlations between the inter-cycle parameters and OR are drawn.

2 Experimental Facilities

Experiments were conducted with a modern 6-cylinder inline, turbocharged, aftercooled, common-rail Cummins diesel engine (ISBe22031), typical of those used in buses or medium sized trucks. Figure 1 shows a detailed schematic of the engine setup along with the pressure and crank angle data acquisition system. Each cylinder has two inlet and two exhaust valves. Cylinders two to five share their inlet ports with their adjacent cylinders while cylinders one and six each have one of their inlet valves supplied by a separate inlet port directly from the inlet manifold because they only have one adjacent cylinder each to share with. More information about the engine specifications can be found in Table 1.

The engine was coupled to an electronically controlled hydraulic dynamometer with load applied by increasing the flow rate of water inside the dynamometer housing. In-cylinder pressure was measured by a Kistler (6053CC60) piezoelectric transducer with a Data Translation (DT9832) simultaneous analogue-to-digital converter connected to a desktop computer running National Instruments LabView. Data was collected at a sample rate of 200 kHz for 1 min at each setting. The fuel injection timing was controlled by the engine management system. Crank angle information and engine speed were acquired from a Kistler crank angle encoder set (type 2614), with a resolution of 0.5 degrees of crank angle. The engine controller is employed to set up the desired engine speed and load as well as record series of working parameters including: brake power, air and fuel consumption, fuel rail pressure, gas emissions, and exhaust and coolant temperature. Readers can find more specific details of the engine setup and modeling methods in [24].

3 Fuel Selection

Four biodiesels (C810, C1214, C1618, and C1875) covering a range of iodine numbers and saponification values were tested here along with commercial diesel. Selected properties of these fuels are shown in Table 2. The first two biofuels (C810 and C1214) have close iodine values (1 and 8) but different saponification numbers (330 and 233) while the other two (C1618 and C1875) have different iodine values (65 and 105) but close saponification numbers (195 and 185). The differences in iodine values and saponification numbers represent the difference in unsaturation degree and carbon chain length of the

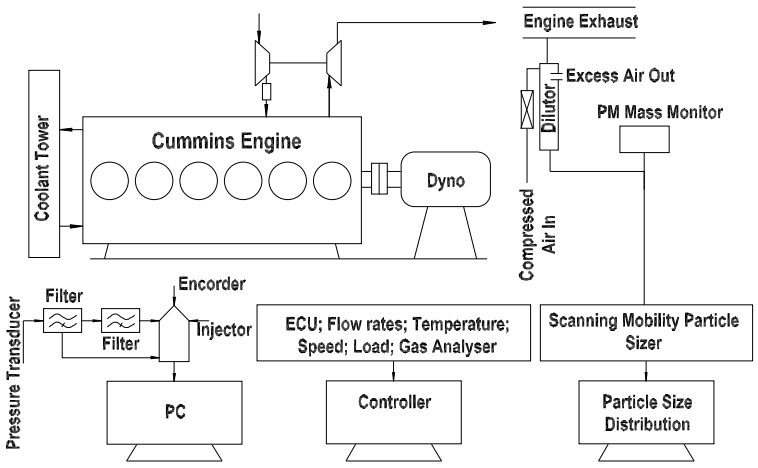

Fig. 1. Schematic of Experimental Setup

Table 1
Experimental Engine Specifications

Manufacturer	Cummins
Serry	ISBe220 31
Number of Cylinders	6
Valves/Cylinder	4
Injection Type	High-Pressure Common-Rail
Bore x Stroke [mm]	102 x 120
Swept Volume [liter]	5.9
Max. Power [kW]	162 (at 2500 rpm)
Max. Torque [Nm]	820 (at 1500 rpm)
Compression Ratio	17.3:1
Dynamometer Type	Hydraulic
Emission Standard	Euro III

biofuels, respectively. Pure biodiesels (B100) as well as blends of 20% (B20) and 50% (B50) by volume with commercial diesel were tested at two speeds (1500 rpm and 2000 rpm) and four loads (25%, 50%, 75%, and 100% of full load). These, along with the base case of pure commercial diesel, result in a comprehensive matrix of tests.

It should be noted that oxygen concentration, average numbers of carbon and hydrogen atoms, stoichiometric air fuel ratios, and heating values listed in Table 2 are estimated using pure substance compositions (supplied by the man-

ufacturer). The reader can consult an earlier paper [25] for more details about these fuels and their properties. The oxygen content of a single methyl ester is easy to calculate from its chemical formulae. For example, methyl octanoate, C8:0 contains approximately 22% of oxygen by mass in its molecule, but the proportion is only 14% for methyl myristate, C14:0 and reduces to 11.2% for methyl stearate, C18:0. An increase in unsaturation level, however, results in a slight increase in the oxygen content. Methyl oleate, C18:1 contains 11.3% of oxygen by mass while methyl linoleate, C18:2 and methyl linolenate, C18:3 contain 11.4% and 11.5% of oxygen, respectively. For the multi-component biofuels fuels used here, the computed oxygen content decreases from C810 to C1875 as shown in Table 2.

Table 2
Selected properties for the fuels studied in this paper

Fuel		C810	C1214	C1618	C1875	Diesel
Iodine value		1.0 max	8	65	105	–
Saponification number		330	233	195	185	–
Rel. density, at 20^{o}C	[kg/m^3]	0.877	0.871	0.873	0.879	0.848
Chemical compounds						
Hexanoic, C6:0	[wt%]	6.0 max	–	–	–	–
Formatic, C8:0	[wt%]	55	–	–	–	–
Decanoic, C10:0	[wt%]	42.5	1.0 max	–	–	–
Lauric, C12:0	[wt%]	1.5 max	50	–	–	–
Miristic, C14:0	[wt%]	–	17.5	–	–	–
Palmitic, C16:0	[wt%]	–	11.5	27.5	4.3	–
Stearic, C18:0	[wt%]	–	3	8	2.2	–
Oleic, C18:1	[wt%]	–	15	53	63.5	–
Linoleic, C18:2	[wt%]	–	4.0 max	–	18.9	–
Linolenic, C18:3	[wt%]	–	–	–	9.2	–
Heneicosanoic, C20:0	[wt%]	–	0.5 max	1.5 max	0.4	–
Enoic, C20:1	[wt%]	–	–	–	1.1	–
Average # of C atoms	–	9.5	14.8	18.3	18.7	–
Average # of H atoms	–	19.7	28.3	35.3	35.3	–
Stoi. AFR, by mass	–	11.12	12.05	12.50	12.48	14.5
Oxygen content	[wt%]	19.29	13.47	11.14	10.96	–
Heating Value	[MJ/kg]	35.35	38.66	39.87	38.07	43.4

4 Results and Discussion

As highlighted earlier, the oxygen ratio, OR (defined as the total oxygen atoms in the fuels and oxidizers to the total oxygen atoms required for stoichiometric combustion) is adopted here as a more relevant parameter for characterizing biodiesels and is hence adopted for displaying some of the data reported in the remainder of this paper. The relationship between OR and AFR for the biodiesels and commercial diesel used here is illustrated in Fig. 2. At the same combustion stoichiometry, a reduction in AFR is observed with an increase in the fuels oxygen content. Diesel requires the highest AFR, followed by C1618, C1875, C1214, and then C810. This is consistent with the increasing oxygen content of these fuels from C1875 to C810. Correspondingly, biodiesels usually have lower heating values and lower stoichiometric air fuel ratio compared to that of diesel.

Cycle-to-cycle variability effects are estimated from data points collected over one minute, resulting in approximately 750 and 1000 individual cycle measurements at 1500 rpm and 2000 rpm, respectively. The statistical distributions that are presented throughout this paper are in the form (i) histograms where the frequency of the events are counted (ii) probability density functions where the integral under the curve sums to one, (iii) standard deviation (StDev), and (iv) Coefficient of variation (CoV) which is the ratio of the standard deviation to the mean. These are applied to the various measured parameters and discussed as relevant in the remainder of this paper.

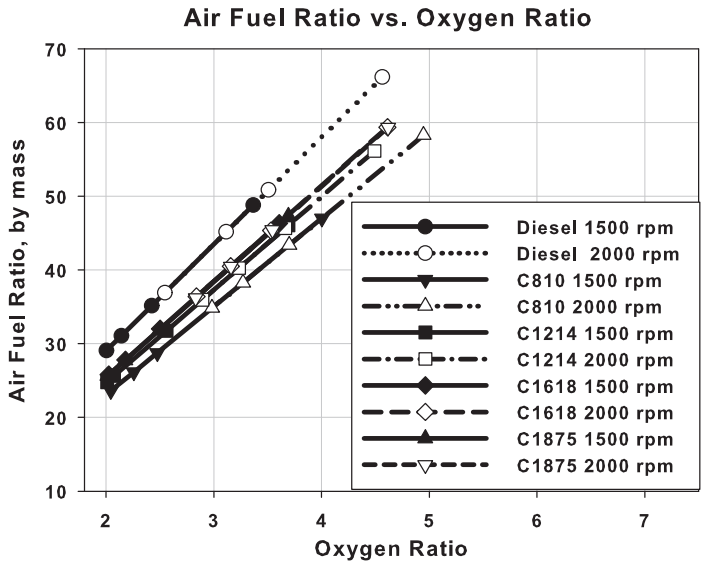

Fig. 2. Air fuel ratio (by mass) of biodiesels and commercial diesel versus oxygen ratio

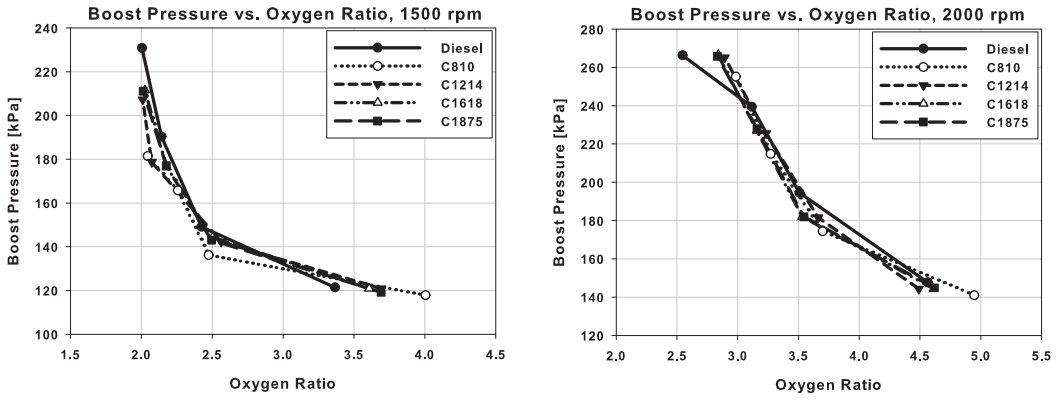

(a) (b)

Fig. 3. Boost pressure of biodiesels and commercial diesel versus oxygen ratio at (a) 1500 rpm; (b) 2000 rpm

4.1 Boost Pressure

Boost pressures measured for all five fuels listed in Table 2 are plotted versus oxygen ratio in Figs. 3a and 3b for 1500 rpm and 2000 rpm, respectively. A somewhat exponential decay of boost pressure is observed with increasing OR and little or no variation is noted between the fuels. This is expected since the boost pressure is theoretically proportional to the flow rate of combustion products through the exhaust. At the same stoichiometry, the total flow rate of fuel and air (and hence the combustion products) varies only slightly between the different fuels; hence, resulting in only a slight variation in the boost pressure.

4.2 Injection Timing and Pressure

The injector is activated by an applied voltage which is recorded and used as the fuel injection signal. Histograms of the start of injection (SoI) are shown in Figs. 4a and 4b for the various fuels with the engine operating at 25% of full load at 1500 rpm and 2000 rpm, respectively. Noting the fine scale on the x-axis, it is evident at a given speed and load, the start of injection is similar for all fuels and occurs generally around TDC (361.4 to 362.4 for all cases shown in Fig. 4). In addition, the fuel injection duration is similar for all fuels and ranges from 25 to 40 DCA at 1500 rpm and from 20 to 35 DCA at 2000 rpm. The higher the engine load, the longer is the injection duration.

The fuel injection pressure was measured by using a rail pressure sensor located at the end of the fuel rail. The injection pressure was observed as a function of engine load and speed. For example, at 1500 rpm the injection pressure was 47 and 61.7 MPa at 25% and 50% of full load, respectively. Similar injection

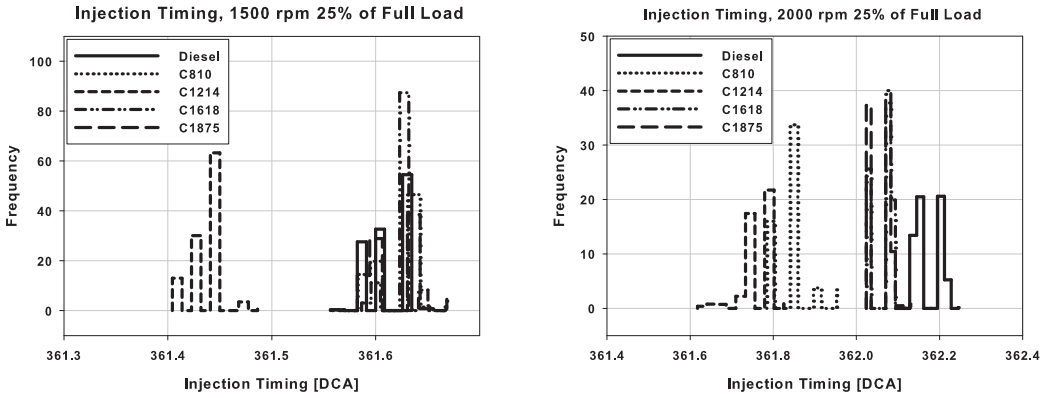

(a) (b)

Fig. 4. Histogram of injection timing of biodiesels and commercial diesel at 25% of full load: (a) at 1500 rpm; (b) at 2000 rpm

pressures of around 75 MPa are also noted at three quarter and full load. At 2000 rpm, the injection pressure at 25%, 50%, 75% and 100% of full load are 63, 80, 87.5 and 97.7 MPa, respectively. Details of the fuel and air flow rates can be made available on request.

4.3 Indicated Mean Effective Pressure (IMEP)

Probability density functions of IMEP measured at full load with an engine speed of 2000 rpm are shown for the range of fuels under investigation in Fig. 5a. Similarly, results are presented for B100, B50, B20 and B0 blends of C810 and commercial diesel at full load and 1500 rpm in Fig. 5b. It is clear from Fig. 5a that diesel yields the highest mean of IMEP followed by two biodiesels, namely C1618 and C1875 both of which have long chain lengths and are partially unsaturated, followed by C1214 which is saturated and has a medium chain length and then C810 which is also saturated but has a short chain length. This decrease in IMEP correlates with the lower heating value of the fuels and hence the oxygen content which decreases significantly with an increase in carbon chain length and a decrease in the degree of unsaturation. The IMEP values of C1618 and C1875 are similar due to the competing effects of carbon chain length and unsaturation degree. As shown in Fig. 5b, there is no significant difference in inter-cycle variation among the biodiesel blends. However, a higher biodiesel proportion in the blend results in a lower IMEP; this being largely due to the constant injection duration.

Figs. 6a and 6b show profiles of the IMEP plotted versus oxygen ratio for all five fuels at 1500 rpm and 2000 rpm, respectively. Similar trends of decreasing IMEP with OR are noted for the commercial diesel as well as the biodiesels and the results are consistent with those presented earlier for the boost pressure in Section 4.1. This also means that, at the same stoichiomet-

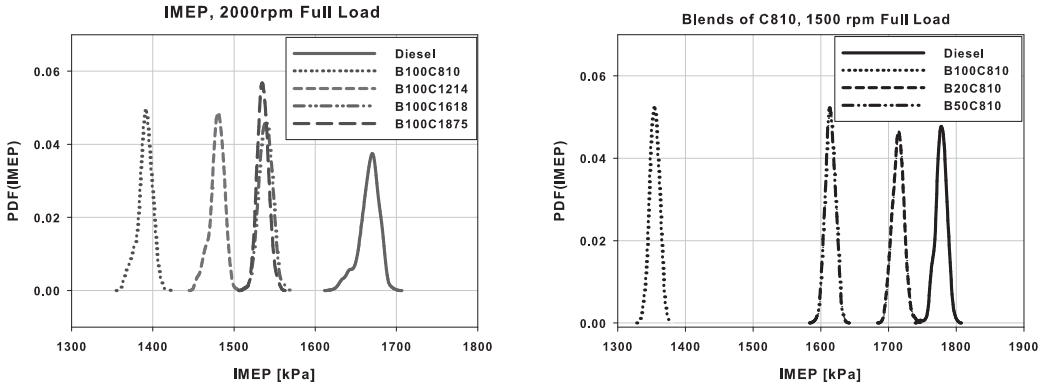

(a) (b)

Fig. 5. PDFs of IMEP at full load (a) Biodiesels and commercial diesel at 2000 rpm; (b) C810 blends at 1500 rpm

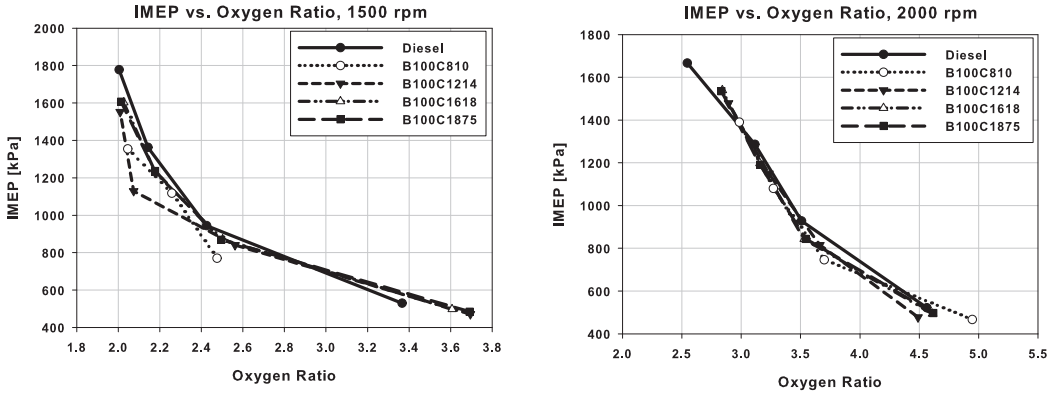

(a) (b)

Fig. 6. Means of IMEP of biodiesels and commercial diesel versus oxygen ratio (a) at 1500 rpm; (b) at 2000 rpm

ric conditions, the higher amount of biodiesels supplied to the engine (due to their lower stoichiometric air-fuel ratio) compensates for the power reductions due to their lower heating values. The consistency between the measured boost pressure and IMEP values is expected since these are global, not local, quantities affected by the total volume of fluid in the combustion chamber.

Two measures of inter-cycle combustion variability of IMEP are shown in Figs. 7a and 7b, one uses single values of the standard of deviation (StDev) plotted versus OR while the other applies kernel density estimates (an estimation of the PDFs), both being for 1500 rpm.

It is clear that the standard deviation of IMEP decreases with increasing OR (or with decreasing engine load) and shows the same trend for all fuels. It can also be seen from Fig. 7a that the values are uniformly small (less than 10 kPa) for diesel fuels as well as biodiesels. Figure 7b shows the PDFs of IMEP for diesel fuel at 1500 rpm but with increasing load from 25% to 100%. It is

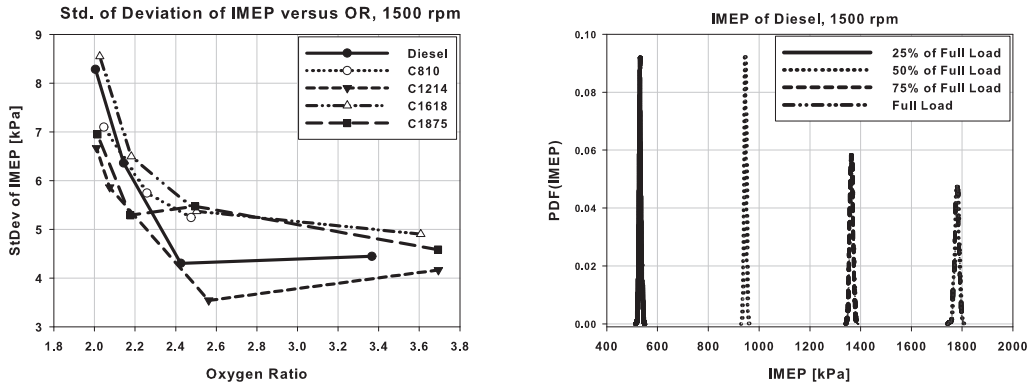

(a) (b)

Fig. 7. (a) StDev of IMEP of biodiesel and commercial diesel versus oxygen ratio at 1500 rpm; (b) PDFs of IMEP of commercial diesel at 1500 rpm

evident from these results that the broadest PDFs, with the lowest peak values, are obtained at full load. This shows that the highest cyclic variations occur at this condition and agrees with the trends evident from the investigation using the single values of standard deviation shown in Fig. 7a. The highest inter-cyclic variability occurring at high loads may be due to the high acoustic excitation in the combustion chamber which results in high fluctuations in the cylinder pressure.

Another single value approach involves using the coefficient of variation (CoV) which is shown in Fig. 8 versus OR for five fuels operating at 1500 rpm (note that only three data points are shown for C810 because the remaining data file was corrupted). It is notable that the effects of engine load on the cycle variability are contradictory between this method and the others using StDev and PDFs shown in Figs. 7a and 7b, respectively. The single value method, using CoV of IMEP in Fig. 8, shows higher variations at low loads, this is attributable the CoV being a normalized value (standard deviation divided by the mean). It is accepted that the CoV of IMEP of compression ignition engines is typically low and the single value method is usually used to analyse the variability for spark ignition engines, which can operate stably with a CoV of IMEP up to 10% [1]. This may suggest that the CoV, on its own, is not appropriate to study the inter-cycle combustion variations in compression ignition engines. It should be used in conjunction with other measures of cyclic variability such as PDFs.

4.4 Net Heat Release Rate (NHRR)

Cycle averaged net heat release rates (NHRR) are obtained from cylinder pressure signals and have been used to analyse several cycle parameters, such as: ignition delay, start and end of combustion, cycle temperature, premixed

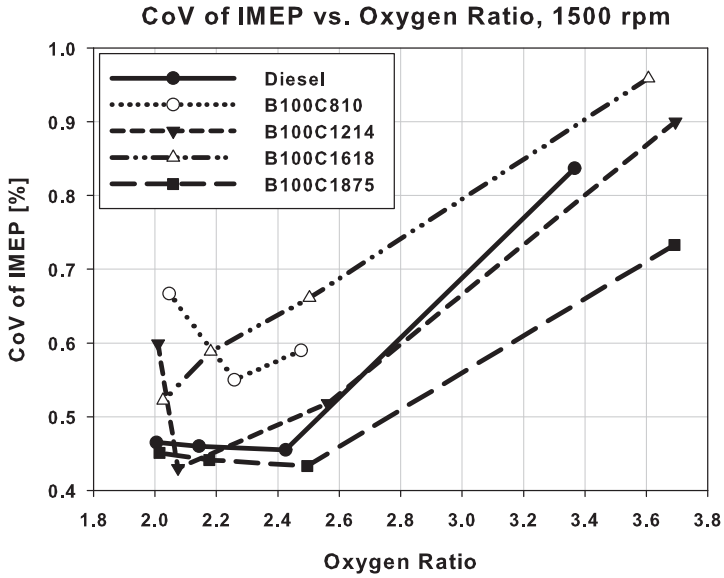

Fig. 8. CoV of IMEP of biodiesels and commercial diesel at 1500 rpm

and diffusion combustion [26,27]. This section examines the influence of engine operating conditions (load and speed) and fuel types on NHRR. Links are made between the combustion characteristics drawn from NHRR information and other cyclic variation parameters such as maximum rate of pressure rise and combustion peak pressure which will be presented in the following sections.

The effects of fuel types (commercial diesel and biodiesels) and engine conditions (speed and load) on NHRR are shown in Figs. 9a and 9b which present results at 1500 rpm and 2000 rpm, respectively. A typical evolution of the heat release is shown, for example, in the results for C810 in Fig. 9a where the NHRR curve presents two separated local peaks, the first one is due to premixed combustion followed by diffusion-type burning during the second peak. It is notable that diffusion combustion, as noted by the highest value of NHRR, peaks around 15-20 DCA after TDC for all fuels at both 1500 rpm and 2000 rpm. Differences in the peak values of NHRR may be attributed to differences between the heating values of diesel and biodiesels.

It can be seen from Fig. 9a that the start of combustion is earliest for C1214 and C1618, followed by diesel and C1875, then C810. This indicates that at these engine modes, the ignition delay of biodiesels increases with a reduction in carbon chain length but reduces with an increase in unsaturation degree. These trends are consistent with those reported by [28] on the influence of FAMEs on ignition delay. At 2000 rpm and 75% of full load (Fig. 9b), the start of combustion seems to occur immediately after the start of injection and premixed combustion is indistinguishable for all fuels. When the engine operates at a higher load and high speed, the cylinder temperature increases so that it is easier for the fuel to ignite resulting in a very short ignition delay.

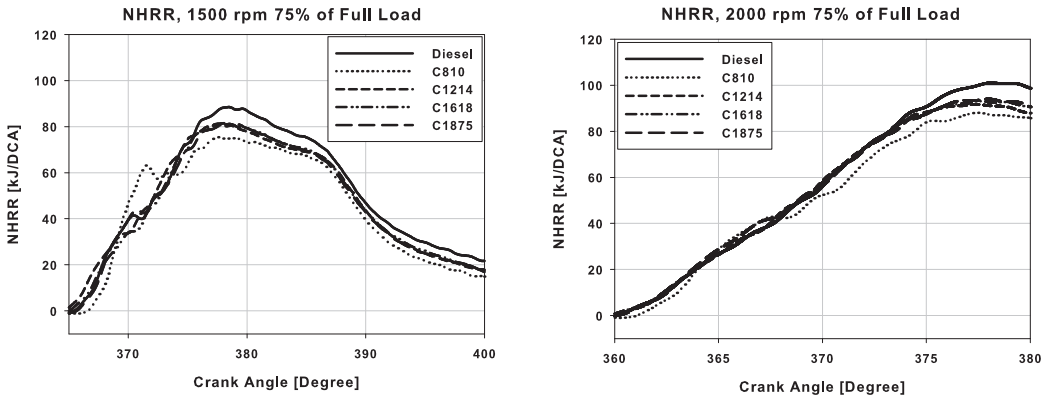

(a) (b)

Fig. 9. Net heat release rate of commercial diesel and Biodiesels (a) at 1500 rpm; (b) at 2000 rpm

At low load, such as 25% of full load shown in Fig. 9b for diesel, the air fuel mixture takes longer time to ignite or longer ignition delay which leads to the distinguishable premixed combustion.

4.5 Motoring and Combustion Peak and the Peak Timing

Motoring and combustion peaks are two typical maximum values in the pressure traces of this Cummins engine. The motoring peak occurs around TDC and this is followed by the combustion peak which is located around 15 to 20 DCA after the motoring peak. It has been reported in earlier work [25] that only motoring peaks can be seen at 2000 rpm and this is attributed to the fact that at this speed, there is a little or no build up of premixing so combustion is dominated by diffusion flames. Therefore, the analysis of motoring and combustion peaks in the following section is performed only at 1500 rpm.

Probability density functions of combustion peak pressure at full load are shown in Fig. 10a and the means of combustion peak pressure are plotted against the engine load n Fig. 10b, for all five fuels at 1500 rpm. It can be seen from Fig. 10a that the means of combustion peak pressure are highest for commercial diesel and lowest for C810, this being consistent with the heating value of the fuel. However, the inter-cycle variability is very similar for all fuels as noted by the similar shapes of the PDFs. It is important to note that at the same load, the trends in the mean of combustion peak pressure are similar to those reported earlier for IMEP. For example, an increase in carbon chain length results in an increase in the mean of combustion peak pressure, however, an increase in unsaturation degree reduces this value. Figure 10b shows similar trends in that, for all fuels and with increasing load, the combustion peak increases, albeit at different rates. While it is known that biodiesels have higher flash points with respect to diesel [28] and this may degrade their

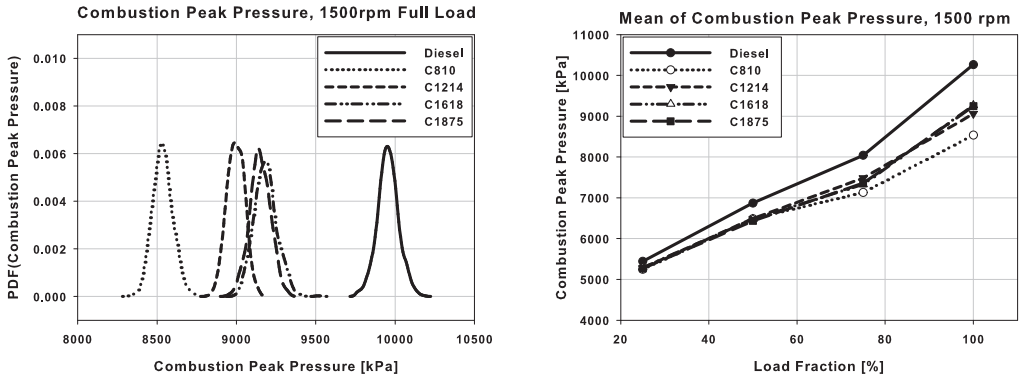

(a) (b)

Fig. 10. (a) PDFs of combustion peak pressure of biodiesels and commercial diesel at 1500 rpm and full load; (b) Means of combustion peak pressure of biodiesels and commercial diesel versus load at 1500 rpm

ignition, measurements of the laminar ignition delays of these fuels would be very useful.

Probability density functions of combustion peak pressure location of biodiesels and diesel are shown in Fig. 11 for all five fuels at 1500 rpm. The combustion peak timing occurs around 15 to 20 DCA after TDC regardless of fuel types. The inter-cycle variability, revealed by the shape of the PDFs are similar for all fuels except C810, which shows much higher combustion variability. This is understandable as C810 has the longest ignition delay and highest premixed combustion proportions; hence, resulting in higher combustion instability.

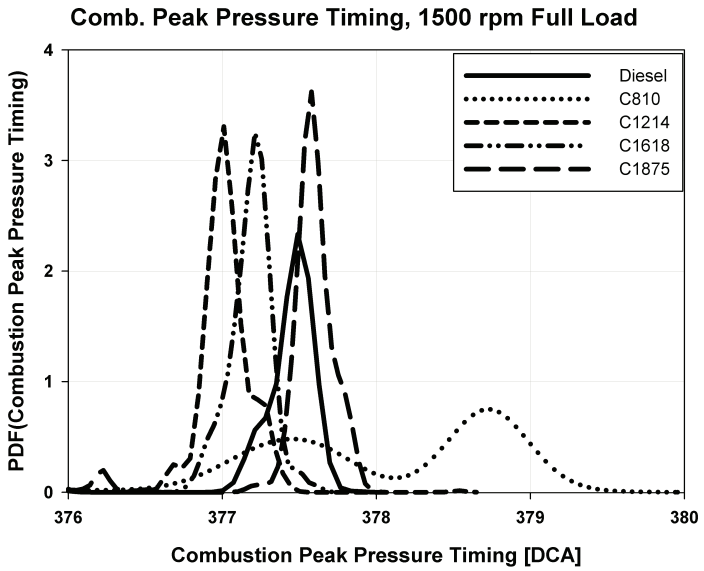

Fig. 11. PDFs of combustion peak pressure timing of biodiesels and commercial diesel at 1500 rpm and full load

Probability density functions of combustion peak pressure are shown in Fig. 12a for blends of C810 with diesel at 1500 rpm and full load while results for

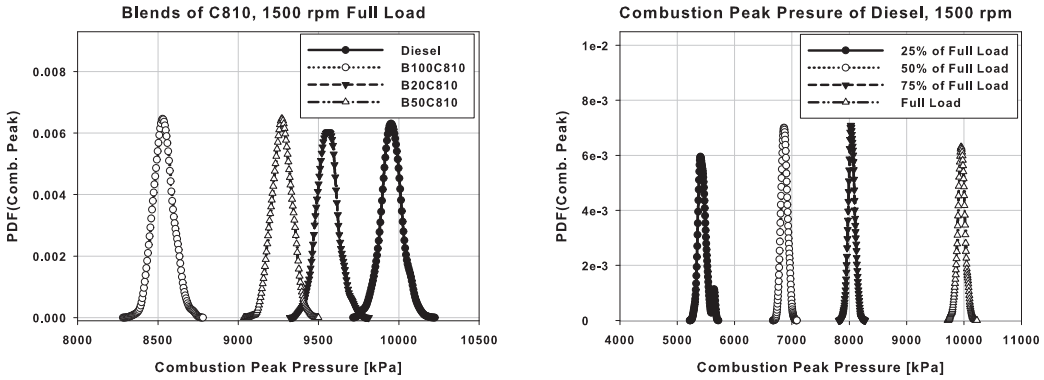

(a) (b)

Fig. 12. PDFs of combustion peak pressure (a) C810 blends at 1500 rpm and full load; (b) commercial diesel at 1500 rpm

different load conditions using commercial diesel at 1500 rpm are presented in Fig. 12b. Both figures highlight the impact of fuel blends and engine load conditions on inter-cycle variations of combustion peak pressure. It is clear from the uniform shape of the PDFs that neither the biodiesel blends nor engine load have significant effects on the inter-cycle variability of the combustion peak pressure. The means of combustion peak pressure, however, increase with a reduction in biodiesel proportions and/or an increase in engine load.

4.6 Maximum Rate of Pressure Rise

The rate of pressure rise is an important parameter that reflects the burning rate of the fuel. Results for the mean peak rate of pressure rise and its PDFs are presented here for a range of fuels at 1500 rpm and 2000 rpm. Fig. 13a shows the PDFs of maximum rate of pressure rise of biodiesels and commercial diesel and Fig. 13b plots the means of maximum rate of pressure rise against oxygen ratio, both are for 1500 rpm. C810 shows the highest mean of maximum rate of pressure rise, followed by diesel then the other biofuels. This is consistent with C810 having the highest proportion of premixed combustion among the current fuels. The inter-cycle variability is also highest for C810 as reflected by the almost flat PDFs shown in Fig. 13b. Conversely, the remaining biodiesels are very similar and show PDFs almost identical to commercial diesel.

Figure 14 shows the PDFs of the maximum rate of pressure rise (Fig. 14a) and the mean maximum rate of pressure rise plotted versus oxygen ratio (Fig. 14b) for the same range of fuels as Fig. 13 but for a higher speed of 2000 rpm. The trends shown at 2000 rpm are remarkably different to those of 1500 rpm. Both the inter-cycle variability of the maximum rate of pressure rise are similar for all fuels. Diesel has the highest mean of the maximum rate, followed by C1618, C1875, and C1214, then C810. The mean peak rates of pressure rise decrease

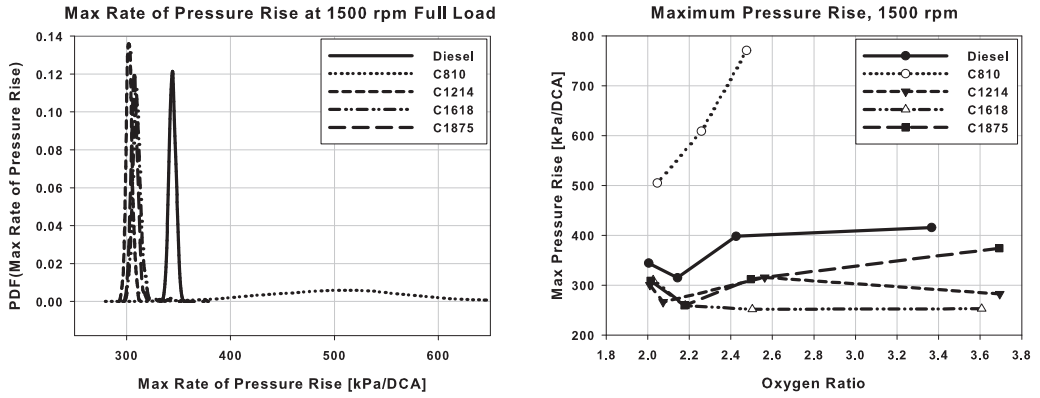

(a) (b)

Fig. 13. (a) PDFs of maximum rate of pressure rise of biodiesels and commercial diesel at 1500 rpm and full load; (b) Means of maximum rate of pressure rise of biodiesels and commercial diesel versus oxygen ratio at 1500 rpm

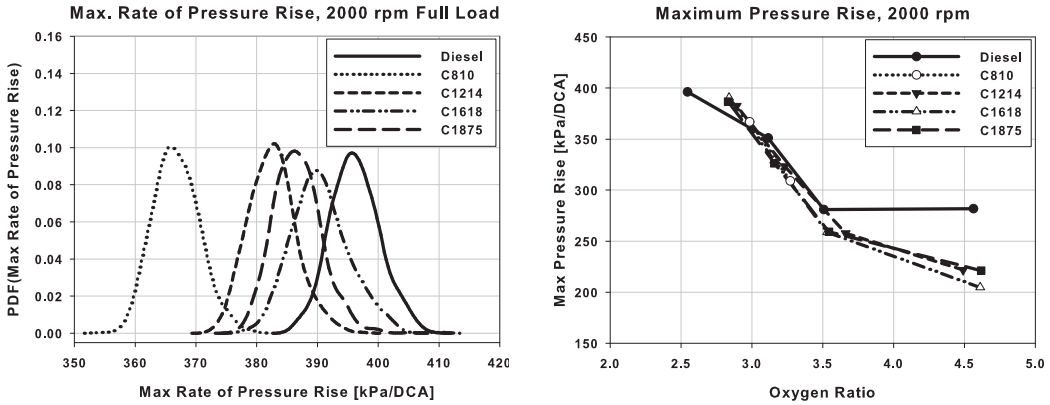

(a) (b)

Fig. 14. (a) PDFs of maximum rate of pressure rise of biodiesels and commercial diesel at 2000 rpm and full load; (b) Mean of maximum rate of pressure rise of biodiesels and commercial diesel versus oxygen ratio at 2000 rpm

with OR and these trends are also similar to those discussed earlier for IMEP. This, however, is not true for 1500 rpm which is shown in Fig. 13a and may be due to the higher effect of premixed combustion proportion which is more dominant at lower engine speed and was found to be highest for C810 fuel.

A significant difference between the two engine speeds can also be seen in the mean of maximum rate of pressure rise shown in Fig. 13b and Fig. 14b. At 2000 rpm and high load conditions, the mean of the maximum rate of all fuels, including commercial diesel, are almost identical (except at high OR where diesel deviates from the rest of the fuels). Significant differences are noted at 1500 rpm and these are most likely linked to differences in the proportions of premixed combustion among the fuels at this low engine speed.

The effect of C810 blends with diesel on inter-cycle variability of the maximum

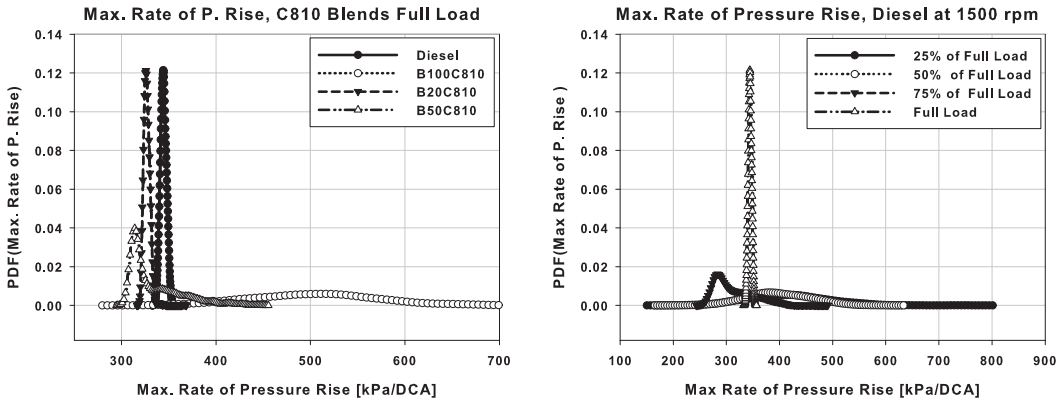

(a) (b)

Fig. 15. (a) PDFs of maximum rate of pressure rise of C810 blends at 1500 rpm and full load; (b) PDFs of maximum rate of pressure rise of commercial diesel at 1500 rpm

rate of pressure rise is shown in Fig. 15a for full load and 1500 rpm. As expected, the variability decreases gradually with increased blending so that commercial diesel and 20% blends are almost identical, as seen from the PDFs shown in Fig. 15a. The effects of engine load on the inter-cycle variability of the maximum rate of pressure rise is shown in Fig. 15b for commercial diesel at 1500 rpm. It is evident that higher loads lead to lower inter-cycle variation of the maximum rate of pressure rise. With the load decreasing from 100% to 75% the increase in variability is significant as reflected by the relevant PDFs shown in Fig. 15b which are broader and have much lower peaks than those obtained at full load. Further reduction and flattening in the PDFs occurs at even lower loads.

4.7 Indicated Specific Particle Mass Concentration (ISPM) and Indicated Specific Total Particle Number Concentrations (ISPM#)

Indicated specific particle mass concentration (in mg/kW h) and indicated specific total particle number concentration (particles/kW h) emitted from biodiesels and commercial diesel are shown versus OR and for 2000 rpm in Figs. 16a and 16b, respectively. Diesel produces the highest particle concentration and C810 the lowest. A reduction in chain length from C1214 to C810, for example, helps to reduce the mass (Fig. 16a) and number concentration (Fig. 16b) by up to 65% at an oxygen ratio of 4.5. The differences in particle concentration of C1618 and C1875 are affected by both carbon chain length and unsaturation degree. The longer carbon chain length of C1875 results in a higher emission of particles, however, its higher unsaturation degree leads to lower particle concentration compared to that of C1618. The oxygen-bound in the oxygenated fuels may contribute to their particle concentration reduc-

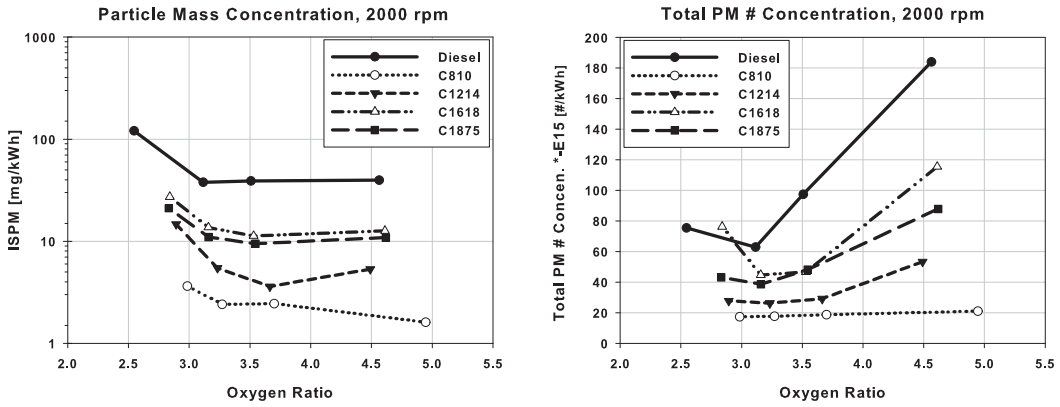

(a) (b)

Fig. 16. (a) Indicated specific particle mass concentration of biodiesels and commercial diesel at 2000 rpm; (b) Indicated specific total particle number concentration of biodiesels and commercial diesel at 2000 rpm

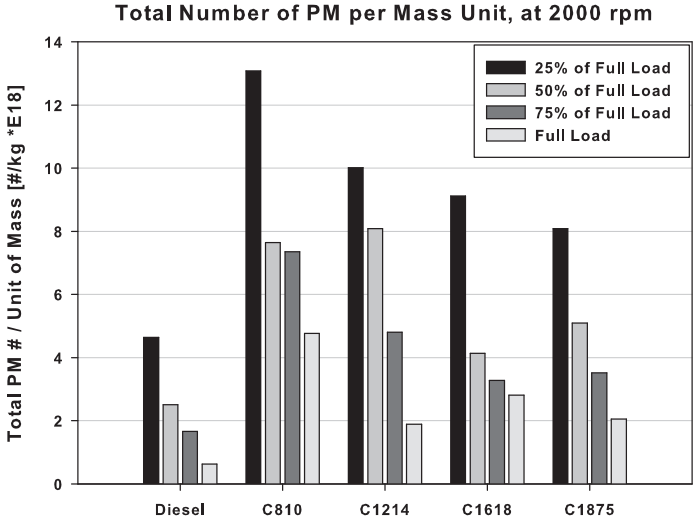

Fig. 17. Number of particle per unit mass of biodiesels and commercial diesel at 2000 rpm

tions, the oxygen content also increases with a decrease in the carbon chain length and/or in unsaturation degree as mentioned earlier. In sum, it is evident that with the utilization of biodiesels in compression ignition engine, a key to minimize the specific particle concentrations (both mass and number) is to reduce the carbon chain length and/or increase the unsaturation degree.

The fractal nature of soot has been reviewed and studied extensively by others [29–31] and several parameters are used in these analyses including gyration radius, particle radius, number of primary particle, the fractal dimension and pre-factor [29]. While a detailed study of fractals is not presented here, the total number of particles per unit mass is used as a lose indicator of fragmentation and this is shown in Fig. 17. As can be seen from Fig. 17 that the fuel

types as well as the engine load have significant effects on the total number per mass unit. At 25% of full load, the indicator is 3 to 5 times higher than that at full load. Also, at 25% of full load, the indicator for diesel is around one half to one third those of the biodiesels. This implies soot fragmentation is more pronounced with biodiesels and is enhanced with a reduced chain length and unsaturation degree. It is evident that the total number of particles per unit mass increases with biodiesels as it correlates with the oxygen content in the fuels, as well as fuel-air mixtures.

5 Conclusion

The effects of the structure of fatty acid methyl esters on inter-cycle combustion variability is analyzed here using a modern six-cylinder inline, turbocharged, aftercooled, common-rail engine. The biodiesels used covered a range of carbon chain length and unsaturation levels. The following conclusions are drawn:

1. The cyclic variability in the combustion peak pressure timing and the maximum rate of pressure rise was similar for all fuels except for C810 and only at low rpm where higher cyclic variability was obtained. This is due to the long ignition delay of this fuel (C810) which leads to higher proportion of premixing. For IMEP, the inter-cyclic variability was similar for all fuels and tends to increase at higher engine loads.

2. While the overall patterns of net heat release rates are similar, differences exist between the different fuels because of variations in the heating values and ignition delays. The second peak in NHRR occurs during the diffusion mode of combustion, 15 to 20 DCA after TDC regardless fuel type. The first peak in NHRR which refers to premixed combustion and this is most distinct with C810 fuel.

3. The emission of particles is strongly affected by the fuel composition. The specific particle concentrations (both mass and number per unit power output) from biodiesels is lower than commercial diesel and decreases with decreasing carbon chain length and/or increasing degree of unsaturation. However, the number of particles per unit of emitted particle mass is higher for biodiesels compared to commercial diesel. High oxygen content in the fuel and short carbon chain length (such as C810) results in a higher number of particles per unit mass.

6 Acknowledgment

This research is supported by the Australian Research Council. The authors would like to thank Mr. M. Rahman, Ms. S. Stevanovic, Mr. M. Babaie, Mr. A. Pourkhesalian, Mr. M. Islam, Mr. J. Islam, and Dr. H. Wang for assistance with the experiments. The support of QUT technical staffs, Mr. N. Hartnett and Mr. Scott Abbet are greatly appreciated.

References

[1] J. Heywood, Internal Combution Engine Fundamentals, McGraw-Hill Book Company, 1988.

[2] A. Sen, R. Longwic, G. Litakc, K. Gorski, Analysis of cycle-to-cycle pressure oscillations in a diesel engine, Mechanical Systems and Signal Processing 22 (2008) 362373.

[3] K. Bizon, S. Lombardi, G. Continillo, E. Mancaruso, B. Vaglieco, Analysis of diesel engine combustion using imaging and independent component analysis, Proceedings of the Combustion Institute 34 (2013) 2921–2931.

[4] J. Bittle, B. Knight, T. Jacobs, Biodiesel effects on cycle-to-cycle variability of combustion characteristics in a common-rail medium-duty diesel engine, in: SAE Technical Paper 2010-01-0867, 2010.

[5] M. Selim, Effect of engine parameters and gaseous fuel type on the cyclic variability of dual fuel engines, Fuel 84 (2005) 961–971.

[6] D. Kouremenos, C. Rakopoulos, K. Kotsos, A stochastic-experimental investigation of the cyclic pressure variation in a di single-cylinder diesel engine, International Journal of Energy Research 16 (1992) 865–877.

[7] M. Selim, M. Radwan, H. Saleh, Improving the performance of dual fuel engines running on natural gas/lpg by using pilot fuel derived from jojoba seeds, Renewable Energy 33 (2008) 1173–1185.

[8] M. A. Portnoff, D. A. Purta, M. A. Nasta, J. Zhang, F. Pourarian, J. R. C., Production of biofuels (2004).

[9] C. Kalra, S. Gangopadhyay, S. Nahar, Environmental aspects of biofuels in road transportation, Environmental Chemistry Letters (2009) 289–299.

[10] J. Gerpen, B. Shanks, R. Pruszko, D. Clements, G. Knothe, Biodiesel production technology, Tech. rep., The US National Renewable Energy Laboratory (2004).

[11] M. Lapuerta, O. Armas, J. Rodrguez-Fernandez, Effect of biodiesel fuels on diesel engine emissions, Progress in Energy and Combustion Science 34 (2008) 198–223.

[12] J. Gerpen, C. Peterson, C. Goering, Biodiesel: An alternative fuel for compression ignition engines, in: Agricultural Equipment Technology Conference, 2007.

[13] Y. Chisti, Biodiesel from microalgae, Biotechnology Advances 25 (2007) 294–306.

[14] A. Dermirbas, Algae as a New Source of Biodiesel, Springer, 2011.

[15] C. Mueller, M. Musculus, L. Pickett, W. Pitz, C. Westbrook, The oxygen ratio: A fuel-independent measure of mixture stoichiometry, 30th International Symposium on Combustion.

[16] G. Ban-Weiss, J. Chen, B. Buchholz, R. Dibble, A numerical investigation into the anomalous slight nox increase when burning biodiesel; a new (old) theory, Fuel Processing Technology 88 (2007) 659–667.

[17] B. Moser, A. Williams, M. Haas, M. Robert, Exhaust emissions and fuel properties of partially hydrogenated soybean oil methyl esters blended with ultra low sulfur diesel fuel, Fuel Processing Technology 90 (2009) 1122–1128.

[18] K. Varatharajan, M. Cheralathan, Influence of fuel properties and composition on nox emissions from biodiesel powered diesel engines: A review, Renewable and Sustainable Energy Review 16 (2012) 3702–3710.

[19] K. Schmidt, J. Gerpen, The effect of biodiesel fuel composition on diesel combustion and emissions, SAE Int. 961086.

[20] C. Lin, S. Lin, Effects of emulsification variables on fuel properties of two- and three-phase biodiesel emulsions, Fuel 86 (2007) 2010–2017.

[21] D. Qi, H. Chen, L. Geng, Z. Bian, Experimental studies on the combustion characteristics and performance of a direct injection engine fueled with biodiesel/diesel blends, Energy Convers Manage 51 (2010) 2985–2992.

[22] M. Lapuerta, O. Armas, R. Ballesteros, J. Fernandez, Diesel emissions from biofuels derived from spanish potential vegetable oils, Fuel 84 (2005) 773–780.

[23] W. Yuan, A. Hansen, M. Tat, J. Gerpen, Z. Tan, Spray, ignition and combustion modeling of biodiesel fuels for investigating nox emissions, Trans ASAE 48(3) (48) (2005) 933–939.

[24] T. Bodisco, R. Brown, Inter-cycle variability of in-cylinder pressure parameters in an ethanol fumigated common rail diesel engine, Energy 52 (2013) 55–65.

[25] P. Pham, T. Bodisco, S. Stevanovic, M. Rahman, H. Wang, Z. Ristovski, R. Brown, A. Masri, Engine performance characteristics for biodiesels of different degrees of saturation and carbon chain lengths, SAE Int. J. Fuels Lubr. 6(1) (2013) 188–198.

[26] J. Sun, J. Caton, T. Jacobs, Oxides of nitrogen emissions from biodiesel-fuelled diesel engines, Progress in Energy and Combustion Science 36 (2010) 677–695.

[27] W. T. Lyn, Study of burning rate and nature of combustion in diesel engines, Proceedings of the Combustion Institute 9 (1962) 1069–1082.

[28] G. Knothe, J. Krahl, J. Gerpen, The Biodiesel Handbook, AOCS Press, 2010.

[29] J. Yon, R. Lemaire, E. Therssen, P. Desgroux, A. Coppalle, K. Ren, Examination of wavelength dependent soot optical properties of diesel and diesel/rapeseed methyl ester mixture by extinction spectra analysis and lii measurements, Applied Physics B: Lasers and Optics 104 (2011) 253271.

[30] T. Bond, R. Bergstrom, Light absorption by carbonaceous particles: An investigative review, Aerosol Science and Technology 40 (2006) 27–67.

[31] C. Sorensen, Light scattering by fractal aggregates: A review., Aerosol Science and Technology 35 (2001) 648–687.